Chapter 2

Higher signal harmonics and increased mass reach of LISA for detection of super-massive black hole binaries

2.1 Introduction

2.1.1 Harmonic content of gravitational waves and various search templates

The GW polarisations of ICB are, at any given PN order, a linear combination of a finite number of harmonics of the orbital frequency. At the Newtonian order, there is a single harmonic, at twice the orbital frequency. At higher orders, the fundamental as well as higher harmonics start to appear. Since the amplitudes of the higher harmonics contain higher powers of the PN expansion parameter, relative to the Newtonian order, they are referred to as amplitude corrections. The phase of each harmonic, determined by the orbital phase, is known upto 3.5PN order (for non-spinning systems[32, 71]).

Motivated by the fact that matched filtering is more sensitive to the phase of the signal than its amplitude [72], search algorithms so far have deployed a waveform model involving only the *dominant harmonic* (at twice the orbital frequency), although the phase evolution itself is included upto the maximum available post-Newtonian (PN) order. Such waveforms, in which all *amplitude corrections* are neglected, but the *phase* is treated to the maximum available order, are called *restricted waveforms* (RWF) and these are what are used so far in the analysis of data from ground-based detectors [73, 74, 75, 76] and also simulated searches for the planned Laser Interferometer Space Antenna (LISA) [51]. Waveforms obtained by including all the known amplitude corrections (upto 2.5PN order for non-spinning systems [77], at the time of writing) are referred to as *full wave forms* (FWF)[1]. In this chapter, we will consider the advantages of the FWF over the RWF in the *detection* of gravitational waves, specifically in the context of LISA.

[1] Subsequent to this work the FWF has been extended to 3PN order. See chapter 4.

2.2 Full WaveForm as search templates for ground-based detectors

In this section, we briefly review the enhanced mass reach of amplitude corrected FWFs, in the context of ground based detectors, specifically Advanced LIGO. Early investigations on the importance of amplitude-corrections for search templates were carried out by Sintes and Vecchio [78, 79]. Their study used only the first-order correction at 0.5 PN order. They concluded that the addition of the amplitude terms in the waveform did not improve the accuracy in the estimation of source's angular position and the distance, whereas the estimation of the chirp and reduced masses could be 10 times better when compared to the RWF. The effect of 2PN amplitude corrections on parameter estimation was studied by Hellings and Moore [80], but specifically in the context of LISA and without discussing the effect of higher harmonics on detection rates for systems with various masses. Recently, in the context of ground-based detectors, Van Den Broeck and Sengupta [81, 82, 83] examined the implications of going beyond the restricted PN approximation and employing instead the full waveform [84, 77]. The two main implications of the comprehensive analysis in Refs. [81, 82] for terrestrial GW detectors may be summarized as follows:

1. For binary neutron stars and stellar mass black holes, restricted waveforms overestimate the SNR as compared the full waveform.

2. The use of the full waveforms significantly increases the mass-reach of second and third generation detectors, Advanced LIGO being able to observe systems with total mass $\sim 400M_{\odot}$ and EGO, a third generation detector as high as $10^3 M_{\odot}$. Thus, for advanced ground based detectors, use of the FWF has significant astrophysical importance in view of the growing evidence of intermediate mass black holes.

We represent the results of [81, 82] in a different way in Fig 2.1. This figure shows how successive PN corrections, leading to the introduction of higher harmonics in the template lead to increased mass-reach of the detector.

2.2.1 Supermassive black hole binaries and LISA

There is strong observational evidence for the existence of supermassive black holes (SMBHs) with masses in the range of $10^6 M_{\odot}$–$10^9 M_{\odot}$ (see e.g. Ref. [59] and references therein) in most galactic nuclei [60]. Therefore, mergers of galaxies, as evidenced by high-redshift surveys, should give rise to binaries containing SMBHs. Late stage evolution of a SMBH binary is dictated by the emission of gravitational radiation. The resulting loss of orbital energy and angular momentum would lead to the coalescence of the two holes. Indeed, X-ray observations have revealed the existence of at least one such system that would coalesce within the Hubble time [85]. Gravitational waves (GW) emitted in the process could be detected by the planned Laser Interferometer Space Antenna (LISA) [51].

Observation of SMBH binaries at high redshifts is one of the major science goals of LISA. These observations will allow us to probe the evolution of SMBHs and structure formation [61] and provide an unique opportunity to test General Relativity (and its alternatives) in the strong field regime of the theory [62, 63, 64, 65, 66]. Observing SMBH coalescences with high (100-1000) SNR [64, 65] is crucial for performing all the aforementioned tests.

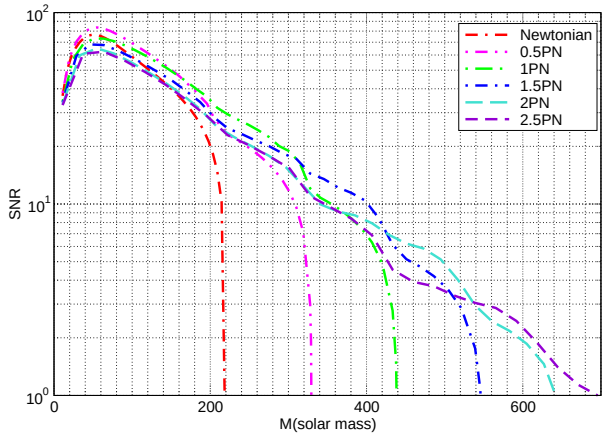

Figure 2.1: Plots of SNR as function of total mass for Advanced LIGO. Distance is fixed at 100 Mpc and mass-ratio is 0.1. The red curve, representing the RWF dominates the SNR at low masses. However, beyond about $220M_\odot$, the SNR due to the RWF goes to zero, while amplitude corrected waveforms are still visible in the detector. Amongst the cases considered, the 2.5PN FWF has the highest mass reach, as it has the highest harmonic among the different waveforms considered. The location and orientation of the source are $\theta = \phi = \pi/6\,, \psi = \pi/4\,, \iota = \pi/3$.

2.2.2 Restricted Vs Full Waveforms as Search templates in LISA

We now consider the advantage of using the *full wave forms* (FWF) in the context of LISA. LISA is designed to detect gravitational waves in the frequency-band 0.1–100 mHz. This frequency range determines the range of masses accessible to LISA because the inspiral regime would approximately end when the system's orbital frequency reaches the mass-dependent last stable orbit (LSO). In the test-mass approximation, the angular velocity $\omega_{\rm LSO}$ at LSO is given by $\omega_{\rm LSO} = 6^{-3/2}M^{-1}$, where M is the total mass of the binary. Search templates that contain only the dominant harmonic cannot extract power in the signal beyond $f_{\rm LSO} = \omega_{\rm LSO}/\pi \simeq 4.39(M/10^6 M_\odot)^{-1}$mHz. This further implies that the frequency range [0.1, 100] mHz corresponds to the range $\sim 4.39 \times [10^4,\ 10^7]M_\odot$ for the total mass of binary black holes that would be accessible to LISA[2]. However, as Table 1 of Ref. [59] would reveal, there is observational evidence for the existence of many SMBHs whose masses are of the order of 10^8–$10^9 M_\odot$. LISA will be *unable* to observe binaries containing SMBHs in this mass range if it used as search templates waveforms containing *only* the dominant harmonic.

Inclusion of higher-order amplitude terms in the waveform introduces the following two new features: (i) appearance of higher harmonics of the orbital phase and (ii) PN amplitude corrections to the leading as well as higher harmonics of the orbital frequency. For example, at 0.5PN order, which is the first-order correction, there are two new harmonics Ψ and 3Ψ, where Ψ is related to the orbital phase of the binary as in Refs. [84, 77]. More interestingly, in the expressions for the 'plus' and 'cross' polarizations, all odd harmonics of the orbital frequency are proportional to $\frac{\delta m}{M}$, where δm is the difference in the masses of the binary components (see Eq. (5.7)-(5.10) of Refs. [77]). Another important feature of the full waveform

[2]Although, binaries lighter than $10^4 M_\odot$ would, in principle, evolve through the LISA band they would not be luminous enough to be visible in LISA unless they are close-by.

is that the $(2n+2)^{\text{th}}$ harmonic first appears at the n^{th} PN order in amplitude[3]. For example, the fourth harmonic first appears at 1PN, and has PN amplitude corrections to its dominant term at 2PN and 2.5PN (see Refs. [77, 84] for details).

In the present chapter, we study in the context of LISA the implication of using templates based on the FWF (i.e. including *all* known harmonics of the orbital phase and *all* known amplitude corrections in the GW polarisations). Coalescences of SMBH binaries with masses $\sim 10^{8-9} M_\odot$ will *not* be observable by LISA if one uses only templates based on the RWF. Using templates based on amplitude corrected full waveforms, instead of the usual restricted waveforms, will enable LISA to observe coalescences of SMBH binaries with total mass $\sim 10^8 M_\odot$ ($10^9 M_\odot$) if the lower frequency cut-off LISA can achieve is $\sim 10^{-4}$Hz (10^{-5}Hz).

The rest of this chapter is organized as follows: In Section 3.3, we give the FWF in the frequency domain, by taking into account the orbital motion of LISA around the sun and its changing orientation. In Section 2.4 we introduce the definition of SNR in the frequency domain and choice of frequency cut-offs. We also discuss about the 'observed' spectrum in LISA for the RWF and the FWF. Section 2.5 discusses the results of our investigations where we compare the performances of the amplitude-corrected waveforms at different PN orders in terms of their mass-reach and distance-reach and correlate it to the 'observed' spectrum in LISA. Section 2.6 concludes with a brief summary of the main results and assumptions underlying their derivation.

2.3 Template waveforms for LISA

2.3.1 Amplitude corrected waveform

For non-spinning binaries in quasi-circular orbits inspiralling due to radiation-reaction, waveforms were computed in Refs. [84, 77] up to 2.5PN order in amplitude and 3.5PN in phase [32, 71]. This waveform $h(t)$ is a linear combination of sine and cosine functions of multiples of the orbital phase $\Psi(t)$. The expression for the 2.5PN polarization contains the first seven harmonics of the orbital phase, the dominant harmonic being the one at twice the orbital phase. The signal depends on the following parameters: D_L, the luminosity distance to the binary, m the total (red-shifted) mass, ν the symmetric mass-ratio (reduced mass divided by total mass), the spherical polar angles (θ, ϕ) determining the direction of the "line-of-sight", the inclination angle ι of the angular momentum $\mathbf{L}$ of the binary with respect to the direction opposite to the line-of-sight, and the polarization angle ψ which determines the orientation of the projection of $\mathbf{L}$ in the plane normal to the line-of-sight.

We rewrite the waveform in terms of only cosines in a form following [82]:

$$h(t) = \frac{2M\nu}{D_L} \sum_{k=1}^{7} \sum_{n=0}^{5} A_{(k,n/2)} \cos[k\Psi(t) + \phi_{(k,n/2)}]\, x^{\frac{n}{2}+1}(t), \tag{2.1}$$

where the coefficients $A_{(k,n/2)}$ and $\phi_{(k,n/2)}$ are functions of $(\nu, \theta, \phi, \psi, \iota)$, and $x(t) = (2\pi M F(t))^{2/3}$ is the post-Newtonian parameter with $F(t)$ the instantaneous *orbital* frequency. Terms $\frac{2M\nu}{D_L} x^{n/2+1}(t)\, A_{(k,n/2)}$ and $\phi_{(k,n/2)}$ are the wave amplitude and polarization phase, respec-

[3]The 0.5PN term is an exception to this and also introduces a harmonic at the orbital frequency apart from the one at thrice the orbital frequency.

tively, corresponding to the k^{th} harmonic and $(n/2)^{\text{th}}$ PN order. We call the coefficients $A_{(k,n/2)}$ the polarization amplitudes. The orbital phase $\Psi(t)$ is a PN series in x, which, in the case of non-spinning binaries, is known to 3.5PN order [32, 71]. For a non-spinning source and a detector whose position and orientation are almost constant during the time of observation of the signal, all the above mentioned angles are constants. For ground-based GW detectors dealt with in Ref. [81, 82], one is in this situation.

2.3.2 Amplitude corrected waveform including modulations due to LISA's orbital motion – Time Domain

LISA will be able to observe many sources from their early stages of inspiral and most would last for a pretty long time. We shall only consider binary sources that last for a year or less before merger. Since the LISA plane is tilted by 60° with respect to the plane of the ecliptic, during the course of its heliocentric orbit (see Fig. 1.5 in Chapter 1) its orientation and position varies periodically, with a period of one year and the signal in Eq. (2.1) will suffer additional amplitude and phase modulations. Thus in the case of LISA the angles θ, ϕ, and ψ (but not ι) appearing in Eq. 2.1 are functions of time. To proceed further, in the frame of a non-rotating observer fixed to the solar-system barycentre, we denote the location of the source on the sky by the spherical polar angles θ_S and ϕ_S and the orientation of the source by the spherical polar angles θ_L and ϕ_L determining the direction of the orbital angular momentum $\mathbf{L}$ of the binary. The transformation between the fixed set of angles[4] $(\theta_S, \phi_S, \theta_L, \phi_L)$ and the time-dependent angular coordinates of the source $(\theta(t), \phi(t), \psi(t), \iota)$ as measured by LISA are given in Ref. [53].

Generalizing, Ref. [53] from the RWF to the FWF, the signal as seen in LISA is of the form,

$$h(t) = \frac{\sqrt{3}}{2}\frac{2M\nu}{D_L}\sum_{k=1}^{7}\sum_{n=0}^{5} A_{(k,n/2)}(t)\cos[k\Psi(t) + \phi_{(k,n/2)}(t) + k\phi_D(t)]\, x^{\frac{n}{2}+1}(t)\,. \tag{2.2}$$

The PN parameter $x(t)$ appearing in Eq. (2.2) is still equal to $(2\pi MF(t))^{2/3}$, where $F(t)$, however, is the orbital frequency as measured by a *non-rotating observer located at the solar-system barycentre*. The term $\phi_D(t)$ is the *Doppler phase* [53], accounting for the phase difference of the gravitational wave-front between LISA and the solar-system barycentre. The time-dependence of $\phi_D(t)$ is due to the orbital motion of LISA about the barycentre. It is given by

$$\phi_D(t) = 2\,\pi\, F(t)\, R\, \sin\theta_S\, \cos[\phi(t) - \phi_S\,], \tag{2.3}$$

where $R = 1$ AU and $\phi(t)$ is the angular position of LISA with respect to the barycentre given by $\phi(t) = 2\,\pi\,\frac{t}{T}$, T being equal to one year.

[4] This is a different notation from [53], where the source angles measured in the fixed barycentre frame are denoted by $(\bar{\theta}_{\rm S}, \bar{\phi}_{\rm S}, \bar{\theta}_{\rm L}, \bar{\phi}_{\rm L})$

2.3.3 Amplitude corrected waveform including modulations due to LISA's orbit – Frequency Domain

The above waveform is valid in the adiabatic regime, where the radiation-reaction time-scale is much larger than the orbital time-scale. We also note that the additional amplitude and Doppler modulations in the waveform for LISA vary on time-scales of 1 yr (i.e. $\sim 3\times10^7$ s), while LISA can observe orbital periods at most up to 2×10^5 s, (i.e. gravitational wave frequencies of order 10^{-5} Hz.). Consequently, the Doppler modulations change much more slowly (a hundredth) than the orbital phase. This permits the use of the stationary phase approximation (SPA) to obtain an analytical form for the Fourier transform (FT) $\tilde{h}(f)$ of the signal:

$$\tilde{h}(f) \simeq \frac{\sqrt{3}}{2}\frac{2M\nu}{D_L}\sum_{k=1}^{7}\sum_{n=0}^{5}\frac{A_{(k,n/2)}(t(f/k))\,x^{\frac{n}{2}+1}(t(f/k))\,e^{-i\phi_{(k,n/2)}(t(f/k))}}{2\sqrt{k\dot{F}(t(f/k))}}\,\exp\Big[i\,\psi_f(t(f/k))\Big], \tag{2.4}$$

where an over dot denotes derivative with respect to time and $\psi_f(t(f/k))$ is given by

$$\psi_f(t(f/k)) = 2\pi f\,t(f/k) - k\,\Psi(t(f/k)) - k\,\phi_D(t(f/k)) - \pi/4. \tag{2.5}$$

The expression for $\psi_f(t(f/k))$ for $k=2$ is given in Eq. (1.56) of chapter 1. The expression in Eq. (3.1) within the summation over k represents the FT due to the $k^{\rm th}$ harmonic. It should be noted that the term $\dot{F}$ may be treated in different ways that could lead to numerically different results. In a numerical treatment, for instance, one could avoid performing a further re-expansion. Alternatively, one could re-expand the denominator in the amplitude and truncate the resulting expression at the $n^{\rm th}$ PN order, to obtain the nPN amplitude-corrected waveform. Ref. [81, 82] choose the latter and we follow them in this work.

Radiation reaction results in an increase in the orbital frequency $F(t)$ which will ultimately drive the system beyond the adiabatic inspiral phase and the inspiral waveform given above will no longer be valid. In the first approximation this is expected to occur when the orbital frequency $F(t)$ reaches $F_{\rm LSO}$ – the orbital frequency of the LSO of a Schwarzschild solution with the same mass as the binary's total mass M,

$$F_{\rm LSO} = (2\,\pi\,6^{\frac{3}{2}}\,M)^{-1}. \tag{2.6}$$

Thus, we truncate the signal in the time domain at a time $t_{\rm LSO}$, given implicitly by $F(t_{\rm LSO}) = F_{\rm LSO}$. In the SPA, the main contribution to the FT of the $k^{\rm th}$ harmonic at a given Fourier frequency f, comes from the neighbourhood of the time when the instantaneous value of the $k^{\rm th}$ harmonic sweeps past f. Thus the $k^{\rm th}$ harmonic is not expected to contribute significant power to the FT for frequencies above $k\,F_{\rm LSO}$, if the signal is truncated in the time domain beyond $t_{\rm LSO}$. This motivates the truncation of the FT due to the $k^{\rm th}$ harmonic at frequencies above $k\,F_{\rm LSO}$ by a step function $\theta(k\,F_{\rm LSO} - f)$ [$\theta(x) = 1$, for $x \geq 0$, and 0 for negative x].

2.4 Signal to noise ratios in LISA with higher harmonics

In this Section we investigate the effect of the higher harmonics in LISA observations of supermassive black hole binaries. The LISA waveform discussed in the previous Section

will be used for the analysis.

Given a waveform h, the best signal-to-noise ratio (SNR) achieved using an optimal filter is given by $\rho[h] \equiv (h|h)^{1/2}$, where $(\,.\,|\,.\,)$ is the usual inner product in terms of the one-sided noise power spectral density $S_h(f)$ of the detector. With the convention for Fourier transforms, $\tilde{x}(f) = \int_{-\infty}^{\infty} x(t)\, \exp(-2\pi i f t)\, dt$, the inner product is given by:

$$(x|y) \equiv 4 \int_{f_s}^{f_{\rm end}} \frac{\mathrm{Re}[\tilde{x}^*(f)\tilde{y}(f)]}{S_h(f)} df. \tag{2.7}$$

For an optimal filter, which maximises the overlap of the signal with template, one can write

$$\rho^2 = 4 \int_{f_s}^{f_{\rm end}} \frac{|\tilde{h}(f)|^2}{S_h(f)} df. \tag{2.8}$$

We use the non-sky-averaged noise-spectral-density as given below.

$$S_h(f) = \min\left\{S_h^{\rm NSA}(f)/\exp\left(-\kappa T_{\rm mission}^{-1} dN/df\right),\ S_h^{\rm NSA}(f) + S_h^{\rm gal}(f)\right\} + S_h^{\rm ex-gal}(f)\,, \tag{2.9}$$

where $S_h^{\rm NSA}(f)$, the instrumental part of the noise, is given by

$$S_h^{\rm NSA}(f) = \left[9.18 \times 10^{-52} \left(\frac{f}{1\ \mathrm{Hz}}\right)^{-4} + 1.59 \times 10^{-41} + 9.18 \times 10^{-38} \left(\frac{f}{1\ \mathrm{Hz}}\right)^{2}\right] \mathrm{Hz}^{-1}\,, \tag{2.10}$$

the galactic white-dwarf confusion noise $S_h^{\rm gal}(f)$ is approximated as

$$S_h^{\rm gal}(f) = 2.1 \times 10^{-45} \left(\frac{f}{1\ \mathrm{Hz}}\right)^{-7/3} \mathrm{Hz}^{-1}\,, \tag{2.11}$$

the contribution from extra-galactic white dwarfs $S_h^{\rm ex-gal}(f)$ is approximated as

$$S_h^{\rm ex-gal}(f) = 4.2 \times 10^{-47} \left(\frac{f}{1\ \mathrm{Hz}}\right)^{-7/3} \mathrm{Hz}^{-1}\,, \tag{2.12}$$

where dN/df is the number density of galactic white-dwarf binaries per unit gravitational-wave frequency, for which we adopt the estimate

$$\frac{dN}{df} = 2 \times 10^{-3}\ \mathrm{Hz}^{-1} \left(\frac{1\ \mathrm{Hz}}{f}\right)^{11/3}\ ; \tag{2.13}$$

$\kappa \simeq 4.5$ is the average number of frequency bins that are lost when each galactic binary is fitted out and $T_{\rm mission}$ is one year. See Ref [62] for more details.

2.4.1 Choice of frequency cutoffs $\mathbf{f_{end}}$, $\mathbf{f_s}$

The upper limit of integration $f_{\rm end}$ is taken to be the minimum of $7\, F_{\rm LSO}$ and 1 Hz, the latter being a conventional upper cut-off for the LISA noise curve. The lower limit f_s is chosen assuming LISA observes the inspiral for a duration $\Delta t_{\rm obs}$ before it reaches the LSO. Using

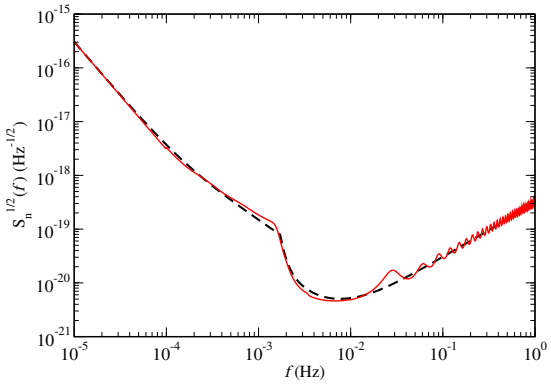

Figure 2.2: Analytic approximation to the *LISA* root noise spectral density curve used in this paper and in Ref. [62] (dashed line) and the curve produced using the *LISA* Sensitivity Curve Generator [86] (solid line). The SCG noise curve does not include the extragalactic white dwarf confusion noise while the analytical approximation curve does.

the quadrupole formula, we find that the orbital frequency at the epoch $t_{\rm LSO} - \Delta t_{\rm obs}$ is given by

$$F(t_{\rm LSO} - \Delta t_{\rm obs}) = \frac{F_{\rm LSO}}{(1 + \frac{256\,\nu}{5\,M}\,\Delta t_{\rm obs}\, v_{\rm LSO}^8)^{\frac{3}{8}}}, \tag{2.14}$$

where $v_{\rm LSO}$ is the orbital velocity and $t_{\rm LSO}$ the epoch at which the orbital frequency reaches the value $F_{\rm LSO}$. We take $v_{\rm LSO} = 1/\sqrt{6}$, the orbital velocity at the LSO in the case of a test mass orbiting a Schwarzschild black hole. We designate $F(t_{\rm LSO} - \Delta t_{\rm obs})$ as $F_{\rm in}$. Thus the $k^{\rm th}$ harmonic will have a frequency $k\,F_{\rm in}$, $\Delta t_{\rm obs}$ before $t_{\rm LSO}$. The above formula reduces to the simpler form in Ref. [62] as $v_{\rm LSO} \to \infty$. For the mass values explored in this work there is no significant dependence of the results on this choice. In all our calculations we take $\Delta t_{\rm obs}$ to be one year.

The lower cut-off for the $k^{\rm th}$ harmonic should be the maximum of the lower cut-off of LISA (10^{-4} Hz) and $k\,F_{\rm in}$ and simply implemented by truncating the waveform due to the kth harmonic by another step-function $\theta(f - k\,F_{\rm in})$ and choosing $f_{\rm s}$ to be 10^{-4}Hz. It is worth noting that the $k^{\rm th}$ harmonic probes a larger interval of the frequency domain i.e. $k(F_{\rm LSO} - F_{\rm in})$ relative to the fundamental harmonic. For brevity, we refer to this as the span of the $k^{\rm th}$ harmonic.

2.4.2 Observed signal spectrum with LISA

To get some insight into the effect of higher harmonics via amplitude corrections let us first look at the SNR integrand, *i.e.*, the "noise-weighted signal power" per unit logarithmic frequency interval [34]. Rewriting the expression for the SNR as

$$\rho^2 \;=\; 4\int_{f_{\rm s}}^{f_{\rm end}} \frac{f\,|\tilde{h}(f)|^2}{S_h(f)} d\ln(f), \tag{2.15}$$

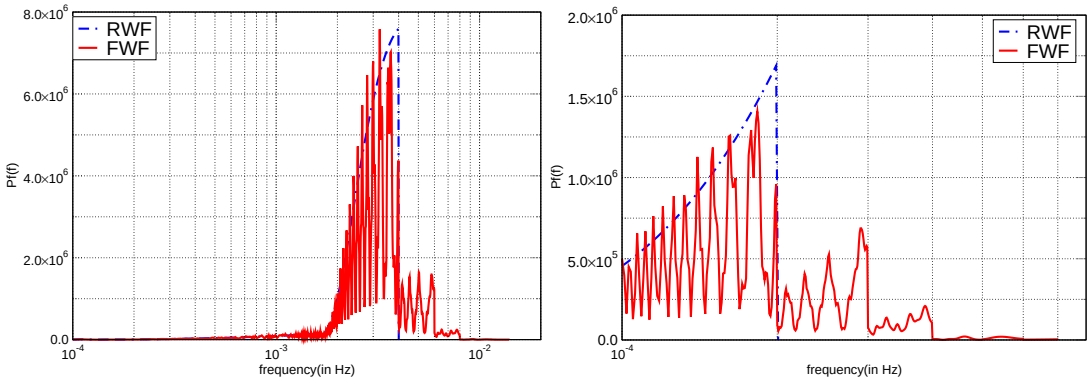

Figure 2.3: The observed spectrum, $\mathcal{P}(f) \equiv \frac{d(\rho^2)}{d(\ln f)} = \frac{f|\tilde{h}(f)|^2}{S_h(f)}$, in LISA using the FWF (solid, red) and RWF (dashed, blue), for sources, $(10^5,\ 10^6)M_\odot$ (left) and $2\times(10^6,\ 10^7)M_\odot$ (right). The sources are assumed to be at 3 Gpc and their angular coordinates w.r.t the solar-system barycentre is $\theta_S = \cos^{-1}(-0.6)$, $\phi_S = 1$, $\theta_L = \cos^{-1}(0.2)$, $\phi_L = 3$. The spectrum is much more complicated and highly oscillatory for the FWF than for the RWF, because of interference between various harmonics. The higher frequency reach of the FWF is due to presence of higher harmonics as apparent in the figure. The spectrum for the system in the left panel sharply rises at a frequency $\sim 2\times10^{-3}$Hz. Beyond this the LISA noise decreases sharply with increasing frequency (fewer galactic binaries per frequency bin) leading to the observed increase in the spectrum.

the quantity of our interest is

$$\mathcal{P}(f) \equiv \frac{d(\rho^2)}{d(\ln f)} = \frac{f|\tilde{h}(f)|^2}{S_h(f)}, \tag{2.16}$$

which is designated as the "observed spectrum", following [83]. The observed spectrum is plotted versus frequency for given masses in Fig. 2.3. As is the case for ground-based detectors [83], the spectrum due to the FWF has a lot more structure and is highly oscillatory because of interference between various harmonics. For the $(10^5,\ 10^6)M_\odot$ system, the mass being low, the second harmonic and hence the RWF extends up to frequencies $\sim 2\times10^{-3}$ Hz, where LISA is most sensitive. This leads to a rapid increase in the observed spectrum in this frequency region. The spectrum due to the FWF, containing higher harmonics continue beyond the RWF into the most sensitive part of the LISA band. For the $2(10^6,\ 10^7)M_\odot$ system, the frequency span of the second harmonic is small and the sensitive region of the LISA band lies beyond its maximum reach.

2.5 The effect of higher harmonics

Following the analysis of Ref. [81, 82], we classify the sources into two types: In the first category are sources for which the dominant (second) harmonic has a large frequency span in the LISA band. The second category on the other hand comprise sources whose dominant harmonic *fails* to enter the LISA bandwidth but the higher harmonics *do*. Since the upper cut-off frequency for each harmonic is inversely proportional to the total mass (from the expression for $F_{\rm LSO}$), we note that the sources of the first type will have total mass less than

Table 2.1: SNRs due to successive PN amplitude-corrected waveforms, with phase corrections to 3.5 PN order in all cases. For the $(10^6 - 10^7)M_\odot$ binary system, all harmonics enter the sensitive part of the LISA bandwidth. Apart from an increase at 0.5PN, we see a consistent reduction in the SNR on inclusion of higher PN order amplitude corrections. For the $(5.5 \times 10^6, 5.5 \times 10^7)M_\odot$ binary system, the second harmonic fails to enter the LISA bandwidth, while the third harmonic spans a small insensitive region. Thus the SNR due to the RWF is zero, while the SNR due to the 0.5PN waveform is smaller than the SNRs due to higher order PN terms. The location, orientation and distance of both sources are the same as in Fig. 2.3.

PN	SNR	
order	$(10^6 - 10^7)M_\odot$	$5.5 \times (10^6 - 10^7)M_\odot$
0	924.48	0
0.5	1025.8	211.98
1	928.48	343.17
1.5	869.78	319.34
2	824.65	266.65
2.5	809.51	277.34

some value which we call the RWF mass-reach, the maximum mass detectable by the RWF, while the second type will have masses greater than this value. The condition that the upper cut-off of the dominant harmonic is less than or equal to the lower cut-off of LISA (i.e., by the inequality $2\,F_{\rm LSO} \leq f_{\rm s}$) determines the RWF mass-reach. The choice of $f_{\rm s}$ for the LISA mission is still not clear and theoretical implications of this choice are explored in e.g. Ref. [87]. For $f_{\rm s}$ in the range $[10^{-5}\,, 10^{-4}]$ Hz the RWF mass-reach varies over the range $[4.39\,, 43.9] \times 10^7 M_\odot$, the lower end of the mass range corresponding to the higher end of the frequency range.

2.5.1 How higher harmonics affect signal visibility

In Fig. 4.2 we plot the SNRs computed using the *restricted* (RWF) and *full* (FWF) waveforms as a function of the binary's total mass for two values of the mass ratio[5]. We first consider systems whose total mass is less than $4 \times 10^7 M_\odot$. For these systems, the SNRs computed using the two different approximations agree with each other to within 10%, with the RWF over-estimating the SNR, when compared to the FWF, in most of the range. This is explicitly shown for a $(10^6,\ 10^7)M_\odot$ binary in the first column of Table 2.1. Indeed, but for the slight increase in SNR as we go from 0PN to 0.5PN, we find a steady decrease as one increases the PN order of the amplitude correction.

The reduction in SNR at higher PN orders can be understood by studying the structure of $|\tilde{h}(f)|^2$, the numerator in the integrand of the SNR in Eq. (2.8). There are basically three types of terms:

[5]Our codes are calibrated by reproducing the results of [81, 82], which considers ground-based detectors, and also of [88], which computes SNRs in LISA using RWF.

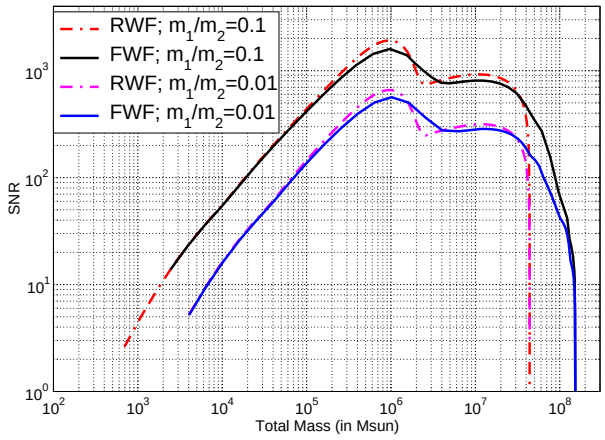

Figure 2.4: SNR versus total mass for mass ratios of 0.1 and 0.01. The figure shows that apart from the dips due to white-dwarf confusion noise, for mass values where the RWF enters the LISA band, the corresponding SNR is consistently more than the SNR produced by the FWF. However, for mass values where the second harmonic terminates before it reaches the LISA bandwidth, the FWF enters the LISA band producing significant SNRs. Since a harmonic's frequency reach depends only on the total mass, the mass reach is independent of the mass-ratio. For more asymmetric systems, the SNR is low for all masses both for the RWF and the FWF. The location, orientation and distance of the sources are the same as in Fig. 2.3.

1. *direct* terms in which the phases in Eq. (3.1) cancel

$$A^2_{(k,n/2)}(t(f/k))\, f^{-\frac{7}{3}}\, (Mf)^{\frac{2n}{3}},$$

2. *interference* terms between *different* PN corrections of the *same* harmonic,

$$A_{(k,m/2)}(t(f/k))\, A_{(k,n/2)}(t(f/k))\, f^{-\frac{7}{3}}\, (Mf)^{\frac{m+n}{3}}\, \cos[\phi_{(k,m/2)}(t(f/k)) - \phi_{(k,n/2)}(t(f/k))]$$

3. *harmonic mixtures*[6] which are terms containing the interference between *different* PN corrections of *different* harmonics, e.g. the $m/2^{\text{th}}$ PN correction of the k^{th} harmonic and $n/2^{\text{th}}$ PN correction of the l^{th} harmonic.

$$A_{(k,m/2)}(t(f/k))\, A_{(l,n/2)}(t(f/l))\, f^{-\frac{7}{3}}\, (Mf)^{\frac{m+n}{3}}\, \cos[\psi_f(t(f/k)) - \phi_{(k,m/2)}(t(f/k)) -$$

$$\psi_f(t(f/l)) + \phi_{(l,n/2)}(t(f/l))]$$

where $\psi_f(t(f/k))$ is given by Eq. (3.2),

All these terms are scaled by $\mathcal{M}^{5/3}$, where $\mathcal{M} = M\nu^{3/5}$ is the chirp-mass. (Additional multiplicative factors have been omitted in the above expressions, among which are the step-functions mentioned earlier and PN expansion coefficients of the denominator of the Fourier amplitude in Eq. (3.1), the latter being time-independent.)

[6]We use the term 'harmonic mixtures' at the risk of being mistaken to the well-known 'harmonic mixing' in music. Our use of the phrase 'harmonic mixtures' is simply to convey the physical effect of the interference between different harmonics

2.5.2 The effect of higher harmonics in ground-based detectors

Before we explain the SNR trends in the context of LISA, we mention that for ground-based detectors a similar effect was found in Ref. [82] for a different but corresponding mass region. The lower cut-off for a typical ground-based detector, say Advanced LIGO is 20Hz, and the effect of higher harmonics is seen for masses less than $\sim 220M_{\odot}$. In that case, as mentioned earlier, the polarisation amplitudes and phases are constants. The RWF contains only the Newtonian term of the second harmonic and thus $|\tilde{h}(f)|^2$ consists of a single direct term with $n = 0$ and $k = 2$.

With the inclusion of higher-order amplitude terms in the waveform, PN corrections to the dominant harmonic and higher harmonics along with their PN corrections, also contribute to the SNR. In other words, the signal power spectrum $|\tilde{h}(f)|^2$ will contain all three types of terms discussed before. From the form of the *direct terms,* it is evident that their contribution to the SNR will be positive definite. We also note that, for ground-based detectors, the frequency dependence of the *direct* and *interference* terms will just be a power law. However, the sign of the interference terms (and consequently their contribution to the SNR) depends on the difference between the polarisation phases of different PN corrections for the same harmonic. Van Den Broeck and Sengupta showed that for a given harmonic, for all allowed values of the parameters $(\nu, \theta, \phi, \psi, \iota)$, each PN correction is almost "out of phase" with *both* the PN correction preceding and succeeding it[7]. The resulting negative terms (representing destructive interferences) reduce the SNR as one includes higher PN amplitude corrections in the waveform.

The third type of terms, harmonic mixtures, however, are highly oscillatory functions of the frequency, as the phase difference $\psi_f(t(f/k)) - \psi_f(t(f/l))$ between the k^{th} and the l^{th} harmonic become even or odd multiples of π. As one integrates over f, these oscillations tend to cancel out, and thus the contribution to the SNR from these terms are numerically much smaller relative to the first two types of terms.

2.5.3 Effect of higher harmonics for binaries with $\mathbf{M < 4 \times 10^7 M_{\odot}}$

In the case of LISA, because of the polarisation factors, the amplitudes of none of the three types of terms is a simple power-law in f. The periodic variation of, for example, $A_{(2,0)}$ (period being one year) appears as an amplitude modulation $A_{(2,0)}(t(f/2))$ in the Fourier transform, where the argument $t(f/2)$ of $A_{2,0}$ is given by

$$t(f/2) = -\frac{5}{256\pi^{8/3}\mathcal{M}^{5/3}}\frac{1}{f^{8/3}} + \text{PN corrections}. \tag{2.17}$$

Hence, in the frequency domain $A_{(2,0)}$ will undergo one complete oscillation as f varies from $2F_{\text{in}}$ (see Eq. (2.14)) to $2F_{\text{LSO}}$. However, because of the *inverse* power-law dependence on f, the oscillation of $A_{(2,0)}$ is confined to a small frequency interval above F_{in} and remains fairly constant over a major portion of the frequency span $2(F_{\text{LSO}} - F_{\text{in}})$ (see Fig. 2.5). For masses higher than the one shown in Fig. 2.5, this region of significant variation moves to the left of the figure. On including in our analysis the effect of detector sensitivity (weighting down by $S_h(f)$) this variation of $A_{(2,0)}$ gets damped out when one evaluates the integral in Eq. (2.8).

[7]Note, however, that Ref. [82], argues this in a somewhat different form.

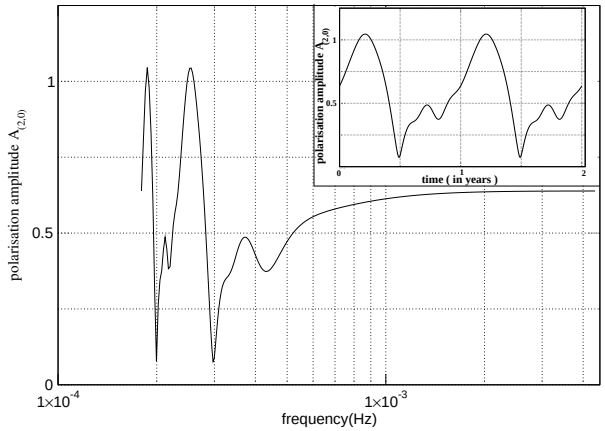

Figure 2.5: Variation of polarisation amplitude of the RWF with frequency and time (inset). The inset, plotted over a duration of two years clearly shows periodicity due to LISA's orbital motion around the Sun. The binary mass, $(10^6 - 10^4)M_\odot$, has been chosen such that it can, in principle, be observed for two years. The plot in the frequency domain shows that the variation of the polarisation amplitude is confined to a very small part of the frequency span of the dominant harmonic, and essentially behaves as a constant in the frequency domain.

For masses satisfying $2F_{\rm in} \ll 10^{-4}$ Hz, the lower cut-off for LISA, this region of variation will fall below the LISA band.

The polarisation phases determining the sign of the interference terms between the same harmonics also vary with f. However, as mentioned earlier, the phase relationships of the polarisation phases are independent of the parameter values. Thus the modulations which change the values of $(\theta, \phi, \psi, \iota)$ do not affect the trend of reduction of SNR with amplitude corrections. The Doppler modulations, which appear in only harmonic mixtures, are also not important as far as SNR is concerned.

Finally, we would like to note an important point not explicitly mentioned in Ref. [82]. As the difference between the polarisation phases of successive PN corrections of the same harmonic tend to be nearly π, alternate PN corrections necessarily interfere constructively. Hence there are positive contributions also from the interference terms. Now, the numerical value of the contribution to SNR from each of these terms depends on the magnitude of the polarisation amplitude and the power of (Mf). It can be checked that for all allowed values of $(\nu, \theta, \phi, \psi, \iota)$, the polarisation amplitudes are roughly of the same order in magnitude. Consider the Newtonian term of the dominant harmonic and its interference with the first two corrections at 1PN and 1.5PN. The Newtonian term will be out of phase with the 1PN term, but in phase with the 1.5PN one. The two corresponding interference terms will contain powers of $(Mf)^{2/3}$ and (Mf), respectively, and since they have the same frequency span, the absolute numerical value of the contribution to SNR from the former will be more since $(2\pi Mf)^{1/3}$ will always be less than $1/\sqrt{6}$. Numerical values of contributions from interference between higher PN corrections of the second harmonic successively decrease. The same argument applies for all the other harmonics, and thus, inclusion of amplitude corrections will lead to an overall reduction in SNR.

The first column of Table 2.1 clearly demonstrates the effect of higher harmonics on SNRs. The increase in SNR for the 0.5PN waveform (with respect the RWF SNR) is also

easily explained by noting that the 0.5PN correction only adds (apart from harmonic mixtures) two direct terms to $|\tilde{h}(f)|^2$, corresponding to the first and third harmonics ($n = 1$, $n = 3$). Clearly, from the discussion in the previous subsection, the 0.5PN waveform will have a higher SNR than the RWF, independent of the binary parameters.

For $10^3 \lesssim M \lesssim 10^5 M_\odot$, the difference between the RWF and the FWF is not visible on the scale of Fig. 4.2 because for this mass range all the direct and interference terms corresponding to harmonics higher than the dominant ones, which are scaled by higher powers of (Mf), are negligible.

2.5.4 Visibility of systems with $\mathbf{M > 4 \times 10^7 M_\odot}$

In their analysis of the implications of the FWF for ground-based detectors Van Den Broeck and Sengupta [81, 82] pointed out an interesting effect due to higher harmonics. An analogous effect is found in the case of LISA in spite of the additional amplitude and Doppler modulations that exist in this case.

Normally, the harmonic at twice the orbital frequency dominates the SNR. However, when the dominant harmonic fails to reach the LISA band the higher harmonics become important, which transpires for masses greater than $4 \times 10^7 M_\odot$. Even though the second harmonic falls below the lower cut-off f_s of the LISA bandwidth, the kth harmonic, $k > 2$, that has power up to a frequency $kF_{\rm LSO}$, might cross f_s and produce a significant SNR. Of course, the kth harmonic would fall below the LISA sensitivity band for masses which satisfy the equality $f_s = kF_{\rm LSO}$. Thus, higher PN order waveforms, which bring in higher harmonics, are capable of producing a significant SNR, even when the RWF fails to produce any.

Let us examine this in a little more detail starting from the values of mass where the second harmonic dominates and the RWF is adequate. Eventually, for larger values of the total mass, the inequality $f_s \geq 3F_{\rm LSO}$ becomes true. Then the 0.5PN waveform, which contains the first and the third harmonic, terminates before reaching f_s and consequently the SNR due to the 0.5PN waveform goes to zero. SNRs for different PN waveforms for a binary whose dominant harmonic falls below f_s and the third harmonic has a small span in the LISA bandwidth is given in the second column of Table 2.1. Note that for the $5.5(10^6 - 10^7)M_\odot$ system, the 1PN waveform has a higher SNR than the 0.5PN one. This is due to the absence of the first harmonic and the small span of the third harmonic in the LISA bandwidth. Further, the 2.5PN waveform has a slightly larger SNR compared to 2PN. This is due to the absence of the first and second harmonic and the small contribution from the third harmonic, all of which contribute interference terms due to their 2.5PN corrections. However, this increase is marginal, and is not generic. We have explicitly checked by choosing different angles that there can be a small decrease also. The detailed results for LISA are summarised in Fig 2.6. We see that for masses for which the 1PN waveform fails to reach the LISA bandwidth, the higher PN order amplitudes are capable of producing SNRs as high as 100! Thus, the use of the FWF will enable LISA to make observations of SMBHs in the astrophysically interesting mass-regime, which would not be possible had one used only the standard RWF.

Using the expression for $F_{\rm LSO}$, it is simple to argue that the mass reach for the 2.5PN FWF, which has the seventh harmonic of the orbital frequency, is $7/2$ times the RWF (around $1.5 \times 10^8 M_\odot$). The above ratio, of course, depends on the assumption that the Schwarzschild (test particle case) LSO frequency will not be very different from the LSO frequency in the

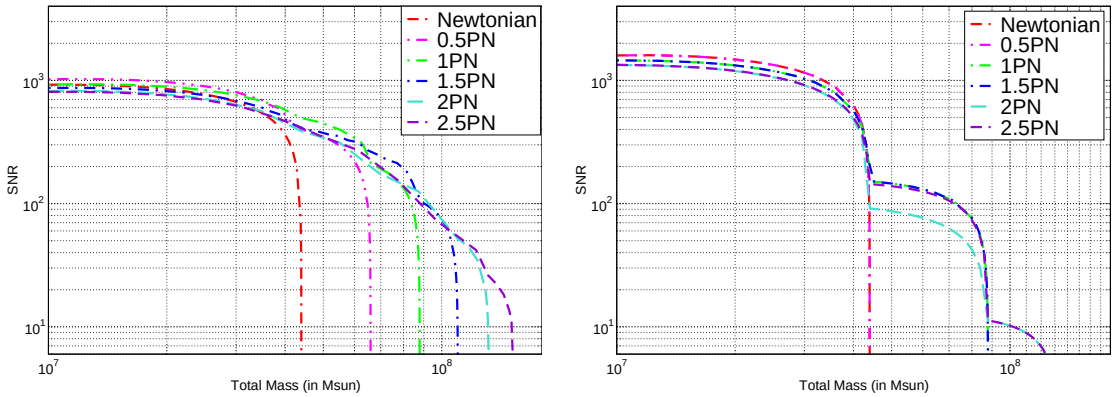

Figure 2.6: SNR versus total mass for successive PN amplitude-corrected waveforms and 3.5PN phasing. The left panel corresponds to a mass-ratio of 0.1 while the right panel plots the same quantities for mass-ratio of 1 (equal mass systems). For a binary of given total mass, the upper cut-off of the k^{th}-harmonic of the orbital frequency in the frequency domain is proportional to k and inversely proportional to the total mass. As the mass increases the upper cut-off for the 2^{nd} harmonic falls below the lower cut-off of the LISA detector, leading to a zero value of SNR due to the RWF. The higher harmonics still enter the sensitive bandwidth of LISA and higher PN order waveforms produce significant SNR. The 2.5PN waveform has the highest mass-reach, being 3.5 times the mass-reach of the RWF. In the equal mass case displayed in the right panel, the differences in harmonic content of different PN order waveforms are more pronounced, as odd harmonics are absent. The location, orientation and distance of both sources are the same as in Fig. 2.3.

comparable mass case.

We conclude with a discussion of a minor, but clear, feature seen in Fig. 4.2 for LISA, but not present for the ground-based detectors, concerning the relative values of the SNR obtained using the RWF and the FWF. For most of the mass range probed the RWF over-estimates the SNR relative to the FWF; however, the figure clearly shows an anomaly for masses around $\sim 2\times 10^6 M_\odot$. To understand this, we first note that the dips in the two curves in Fig 4.2, are due to the bump in the LISA noise-curve [62] just above 10^{-3} Hz. This bump is due to the domination of white-dwarf confusion noise over instrumental noise and lies just below the most sensitive frequency region ($\sim 3\times 10^{-3}$Hz - 2×10^{-2} Hz) of the LISA band. Below 3×10^{-3} Hz, the noise increases sharply till one reaches the bump. For binaries of mass greater than $1.5\times 10^6 M_\odot$, the frequency span of the dominant harmonic ends just around the bump and the sensitive region of the LISA band is beyond the span of this harmonic. However, higher harmonics incorporated in the FWF are able to reach the sensitive part of the noise curve. This leads to higher SNR for the FWF relative to the RWF. This reversal of trend continues up to masses $4\times 10^4 M_\odot$. Above this mass, the frequency span of the seventh harmonic ends before the sensitive region of the LISA band and the general trend is restored.

For still higher mass values, the SNRs due to the RWF and the FWF both increase until the second harmonic fails to reach the LISA band. This is due to the overall scaling of the waveform with the total mass. At such high values, it is able to compensate both for the decreasing frequency span and the higher noise of the detector in this frequency range.

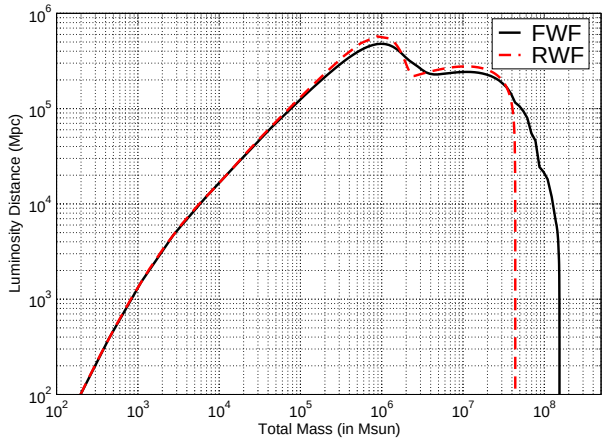

Figure 2.7: Luminosity Distance (in Mpc) versus total mass for a fixed SNR of 10. The systems have mass-ratio of 0.1. The distance reach can be as large as 500 Gpc for systems where the second harmonic enters the LISA bandwidth. Systems undetectable by the RWF (of mass around $10^8 M_\odot$) can be detected by the FWF at distances up to 10 Gpc. The location and orientation of the sources are the same as in the earlier figures.

2.5.5 Effect of higher harmonics in the equal mass case

In contrast to asymmetric systems discussed so far, for systems of equal mass *all* odd harmonics are absent. Consequently, for symmetric systems the mass-reach of the 2.5PN FWF will be only 3 times the mass-reach of the RWF. Further, from the right panel of Fig. 2.6, it is clear that the 0.5PN and the 0PN, or RWF, are identical, as are the 1PN and 1.5PN waveforms. Thus the decrease in SNR for the higher PN order waveforms with increasing total mass is more pronounced than in the unequal-mass case. We also note that for masses for which the second harmonic fails to reach the detector bandwidth, the 2PN waveform has a lower SNR than the 2.5PN waveform. This can be explained by noting that for these masses only the fourth and sixth harmonics enter the LISA bandwidth. The 2PN waveform contains the leading term of the fourth harmonic at 1PN and its 2PN correction, which interfere destructively. However, inclusion of the 2.5PN amplitude correction leads to a constructive interference term between the 2.5PN correction and the 1PN term which is responsible for increasing the SNR for the 2.5PN waveform.

It is interesting to note that the computation of the 3PN GW polarization which will introduce an harmonic at 8Ψ will be quantitatively more significant for the equal mass case as the mass reach will be better by 33% relative to the 2.5PN FWF as opposed to the unequal mass case where it is only 14%! This provides one motivation for work reported in chapter 4 on the computation of the 3PN accurate GW polarizations.

2.5.6 Variation with mass ratio

Since the mass reach depends only on the total mass, the trends remain the same for different values of mass ratios. Fig. 4.2 compares the variation of SNRs with mass for mass ratios of 0.1 and 0.01. If the SNR is dominated by the second harmonic, the SNR is smaller for more asymmetric systems by an overall factor of ν, where $\nu = m_1 m_2/m^2$. However, once the second harmonic fails to reach the sensitive bandwidth of LISA, the more asymmetric

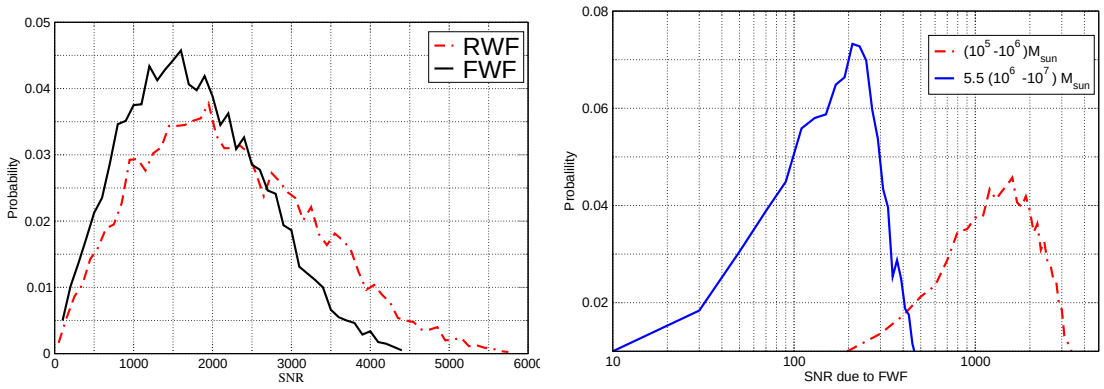

Figure 2.8: Distribution of SNR with sources randomly located and oriented in the sky. The left figure plots SNRs due to both RWF and FWF for a binary of mass $(10^5 - 10^6)M_\odot$. For this mass, the most probable SNR for the FWF is lower than the most probable SNR for the RWF, like the trend shown in Table 2.1. The right figure compares the SNRs due to the FWF for binaries of mass $(10^5 - 10^6)M_\odot$ and $5.5(10^6 - 10^7)M_\odot$

systems have a dominant contribution from the odd harmonics which scale by a further factor of $\sqrt{1-4\nu}$, which is larger for more asymmetric systems. Thus the decrease in SNR for the FWF with an increase in the total mass is less steep for more asymmetric systems.

2.5.7 Distance reach with the 2.5PN FWF

Next, we compare the distance-reach of the RWF and the 2.5PN FWF. The results are shown graphically in Fig. 2.7 and are similar in appearance to the mass-reach plot. The mass-reach of the RWF is $\simeq 4 \times 10^7 M_\odot$. For a system of total mass $5 \times 10^7 M_\odot$, the plot shows that LISA can detect such binaries with an SNR of 10 at a luminosity distance of 100 Gpc ($z \simeq 15$). SMBHs of total mass $\sim 10^8 M_\odot$, not even observable using RWF templates, have a distance-reach as high as 10 Gpc ($z \simeq 1.5$) with an SNR of 10.

Proposals to extend the frequency band-width of LISA up to 10^{-5} Hz have been discussed. In that case, the FWF can increase the mass-reach of LISA to even around $10^9 M_\odot$. More specifically, LISA can then observe a $10^9 M_\odot$ system with an SNR of about 30 at 3 Gpc, if it uses templates based on the 2.5PN FWF for data-analysis.

2.5.8 Sensitivity of SNR to source location and orientation

All the results for SNR using the amplitude-corrected waveforms quoted earlier have been for a fixed choice of location and orientation of the source [defined by the angles$(\theta_S, \phi_S, \theta_L, \phi_L)$] with respect to the barycentre coordinate system. To conclude our present analysis, in this section we look into the variation in the value of SNR for sources at various locations in the sky and various orientations. To this end, we consider a collection of sources randomly oriented in the sky and study the probability distribution of their SNRs. The results of our simulations (consisting of 8000 random realisations of the angles involved) are shown in Fig. 2.8. From the left panel of Fig. 2.8 we see that the most probable SNR due to the FWF for a $(10^5,\ 10^6)M_\odot$ binary is less than the most probable SNR due to the RWF, indicating that this trend is independent of the source location and orientation. In the right panel we see that

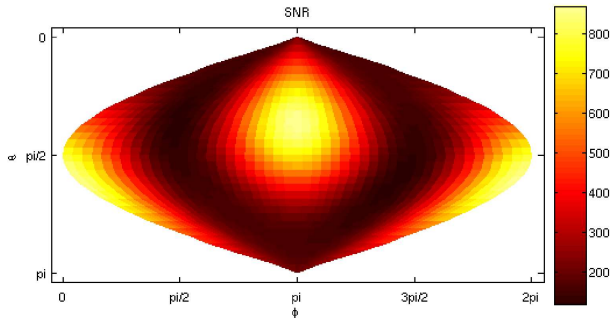

Figure 2.9: Sky map of for LISA observations of the final year of inspirals using 2PN waveform. The sources are equal mass binaries each of mass $10^7 M_\odot$, at $z = 1$, with fixed orientation angles at $\mu_L = 0.2$, $\phi_L = 3$. (Figure reproduced from Ref. [89].)

a binary of mass $2 \times (10^6, 10^7) M_\odot$, which is undetectable by the RWF, can be observed by the FWF with a most-probable SNR of around 220.

Recently, Trias and Sintes [89] have performed all sky simulations of parameter estimation using the 2PN waveform. Even though they have not used the same truncation procedure as us for the $\dot{F}$ term in Eq 3.1, the results qualitatively do remain the same. Here we reproduce from their paper an all-sky map of SNR for an equal mass SMBH binary (Fig(3.1)for a fixed source orientation.

2.6 Summary

The implications of amplitude corrected 2.5PN *full* waveforms (FWF) for the construction of detection templates for LISA are investigated in detail. With the FWF, LISA can observe sources which are favoured by astronomical observations, but not observable with restricted waveforms (RWF). This includes binaries in the mass range $10^8 - 10^9 M_\odot$, depending on whether the lower cut-off for LISA is chosen to be at 10^{-4} Hz or 10^{-5} Hz. With an SNR of 10, these systems can be observed up to a redshift of about 1.5. The computation of the 3PN polarization, which will introduce an harmonic at 8Ψ (i.e. four times the dominant harmonic), in addition to the existing harmonics, could enhance the mass reach for equal mass binaries by 33% and unequal mass binaries by 14.3%.

The implication of the FWF for parameter estimation will be far more important than the extension of LISA's mass-reach reported here. From the work of Van Den Broeck and Sengupta in the context of ground-based detectors [83] it is already clear that most parameters will be estimated with errors $\sim$ ten times smaller as compared to RWF. This raises the interesting possibility that binary SMBH coalescences might be located on the sky with accuracies good enough for optical observations to identify the galaxy cluster and measure its red-shift. Needless to say that this improved estimation of source properties will have important consequences in shedding light on the dark energy, better understanding of SMBH formation and evolution, structure formation, etc., and is currently under investigation.

In this work we have confined ourselves to only non-spinning black-holes ignoring the effect of spin-orbit coupling at 1.5PN [90] and 2.5PN [91] and spin-spin effect at 2PN or-

der [92]. The effect of spin is expected to be astrophysically significant and it is important to revisit the present analysis including spin in the future. Though partial results for GW polarisations including spin do exist, a more exhaustive exercise would be necessary before the FWF required for this work is available. The problem will also be more complicated due to modulations arising from spin-orbit and spin-spin couplings which would need to be addressed.

In this work we also restricted to the inspiral phase and used a physical picture of the LSO that is based on the test-particle limit. For comparable masses, the notion of LSO is not as sharp, or unique, and hence our results are probably idealized limits of the real situation. Numerical relativity [93, 37, 45] is maturing over the past couple of years and could soon provide waveforms for late inspiral and merger. It should then be possible to compare the results of such numerical templates with those studied in this chapter to provide a better understanding of how higher harmonics facilitate the mass reach of our detectors.